

Nonlinear absorption in indium arsenide

K. W. Berryman

Department of Electrical Engineering, Princeton University, Princeton, New Jersey 08540

C. W. Rella

Stanford Picosecond FEL Center, W. W. Hansen Experimental Physics Laboratory, Stanford University, Stanford, California 94305-4085

(Received 29 August 1996)

Using a free-electron laser source, we have studied the nonlinear absorption in indium arsenide at three representative wavelengths: 4.55, 5.06, and 6.30 μm . By measuring the temperature dependence of the two-photon-absorption (TPA) coefficient we have been able to discriminate between parabolic and nonparabolic band models of the TPA process. Using an extension of these methods we were also able to measure the free-carrier absorption induced by TPA and to demonstrate the importance of other higher-order absorption processes. [S0163-1829(97)05212-0]

I. INTRODUCTION

The interaction of photons with carriers in a semiconductor is one of the most studied and technologically useful areas of condensed matter physics.¹ Although linear optical processes are generally well understood and used in a variety of applications, nonlinear interactions have enjoyed increasing interest both because of the recent availability of intense sources and the potential for new devices. Using a midinfrared free-electron laser (FEL), we have studied the nonlinear absorption in indium arsenide in order to measure both the two-photon and free-carrier absorption coefficients with sufficient precision to provide a strong experimental check of present theory. Furthermore, by separating the contributions of these two mechanisms to the nonlinear absorption we are able to observe additional higher-order processes, thereby establishing a framework for exploration of these higher-order absorption mechanisms.

In general, optical absorption in a semiconductor can occur via many routes, each with different dependencies on the incident intensity.² Our approach is, therefore, to obtain careful measurements of the absorption as a function of intensity to separate contributions from different mechanisms. Using measured values obtained from low-intensity data, we are able to fit to higher intensities and thereby observe higher-order processes. Each absorption mechanism can be then be monitored as we change excitation wavelength or sample temperature, resulting in measured absorption coefficients that can be used to validate existing theories.

In a direct band-gap semiconductor, two-photon absorption (TPA), in which two photons together provide the energy for a carrier transition, is usually the first nonlinear absorption mechanism to be of importance. The TPA process results in an absorption proportional to the square of the incident intensity, with constant of proportionality designated the TPA coefficient. Since TPA is masked at wavelengths corresponding to energies greater than the band gap by the linear absorption, observation requires a high-intensity source at the appropriate wavelengths. Conventional laser sources have enabled the study of TPA throughout the visible and near infrared in many semiconductor

systems.³ The tunability afforded by FEL's throughout the mid-infrared has allowed studies of narrow-gap semiconductors. Workers at other FEL centers have studied TPA in InSb, InAs, and $\text{Hg}_x\text{Cd}_{1-x}\text{Te}$, obtaining qualitative agreement with simple theory.⁴⁻⁶ The measurements discussed here have all been performed in the InAs system, and provide not only quantitative comparisons to theory, but also confirmation of predicted nonparabolic contributions to the TPA coefficient.

At higher intensity, the nonlinear absorption observed is greater than that predicted by simple TPA theory. The next-higher-order absorption process is free-carrier absorption (FCA) by TPA produced carriers. Using the TPA coefficient obtained from the optical transmission at moderate intensities, we have been able to measure the FCA cross section over a range of frequencies and temperatures. Furthermore, using the measured TPA and FCA rates to fit data at higher intensities we have been able to demonstrate the importance of higher-order absorption processes.

II. CALCULATION OF TPA RATES

Two-photon absorption is a quantum process with a transition probability that can be calculated with Fermi's golden rule. For a given band structure, carrier wave functions are determined, and matrix elements computed with the optical interaction Hamiltonian. The matrix elements are then summed over all possible transitions to determine the TPA rate.

For single parabolic valence and conduction bands, the calculation is straightforward and results in a TPA coefficient β with functional form⁷

$$\beta(\omega) \propto \frac{F(\hbar\omega/E_g)}{n^2(\omega)E_g^3}, \quad (1)$$

$$F(x) = \frac{(2x-1)^{3/2}}{(2x)^5}.$$

Here n is the index of refraction and E_g is the gap energy. These equations allow one to compute the TPA coefficient as

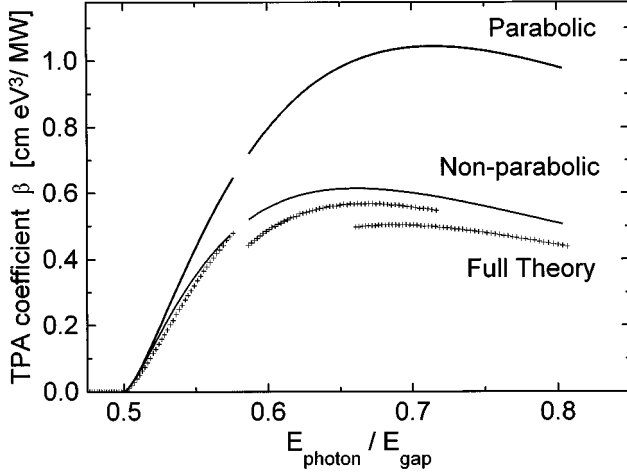


FIG. 1. Theoretical calculation of the two-photon absorption coefficient according to three band structure models: simple parabolic, nonparabolic without split-off band, and a complete model including split-off band. The two simpler models are parametrized by the ratio of the photon energy to band gap, while the full model predicts a separate curve for each wavelength, in this case corresponding to 4.55, 5.06 μ , and 6.3 μ m. At each of these wavelengths, the TPA coefficient has been plotted for temperatures between 80 and 350 K. All three models have been scaled by $E_{\text{gap}}^3 n^2$.

a function of frequency, where F yields the functional form of this dependency. The constant of proportionality in Eq. (1) is determined by the material properties.

A parabolic model, however, is a crude approximation, valid only close to the Brillouin-zone center. More detailed calculations have been performed that include the effects of nonparabolicity of bands and nonzone center wave functions. If the split-off band is ignored, these calculations indicate a spectral dependence of the form⁸

$$F(x) = \frac{(2x-1)^{3/2}}{3x^3} \times \left[\frac{4(3x)^{1/2}}{(3x-1)^2} + (3x+1.5)^{3/2} \frac{(9x^4+10x^2+6)}{90x^5} \right]. \quad (2)$$

A full model must also include transitions from the split-off band. Unfortunately, the spectral dependence for a Kane band-structure model, including the split-off band, cannot be reduced to a compact form like Eq. (2). The full model involves 46 unique matrix elements which must be summed over all possible transitions between two conduction bands (with different electron spin) and six valence bands (light, heavy, and split-off hole for both spin states). The full details of this calculation are given by Hutchings and Van Stryland.⁹

We have extended this calculation to include the temperature dependence of the energy gap. The variation of other band-structure parameters with temperature is of secondary importance and is ignored here. Our calculation is compared in Fig. 1 with the two analytic models discussed above. We have plotted the TPA coefficient here as a function of the ratio of photon energy to energy gap. Since the two simplest models depend only on this ratio, they may be plotted on a

single curve. For the full model, however, separate curves result for each wavelength. In the figure we have plotted calculated TPA coefficients for 4.55, 5.06, and 6.3 μ m which explains the three separate curves for the most complete model.

III. OPTICAL PULSE PROPAGATION WITH NONLINEAR ABSORPTION

To test these theoretical predictions, we would like to measure the dependence of the TPA coefficient as a function of photon frequency and gap energy. One way to measure the TPA coefficient is to observe the nonlinear absorption experienced by an optical pulse traveling through the material. For a general material, the change in intensity experienced by a propagating light wave may be written, to second order in the intensity,¹⁰

$$\frac{d}{dz} I(r,z,t) = -\alpha(r,z,t)I(r,z,t) - \beta(r,z,t)I^2(r,z,t), \quad (3)$$

where both the linear absorption coefficient α and the TPA coefficient β can change during the pulse as a result of either saturation or carrier production. The linear absorption is given by $\alpha = \alpha_0 + \alpha_c(r,z,t)$, where the constant α_0 is the contribution from linear absorption due to impurity and lattice absorption, and $\alpha_c(r,z,t)$ consists of the absorption due to free electrons and free holes, and can be expressed as

$$\alpha_c(r,z,t) = \sigma_n[n_0 + N(r,z,t)] + \sigma_p[p_0 + N(r,z,t)] \quad (4)$$

in which σ_n and σ_p are the absorption cross sections for free electrons and free holes, respectively, and $N(r,z,t)$ is the population of electron-hole pairs created via TPA. The populations n_0 and p_0 are the equilibrium concentrations of electrons and holes, respectively. These bulk concentrations do not depend on position or time, and so can be included in the constant α_0 . Furthermore, since direct intraband carrier transitions can only occur in the valence band, $\sigma_p \gg \sigma_n$, and so we can write

$$\alpha_c(r,z,t) \cong \sigma_p N(r,z,t). \quad (5)$$

Implicit in the above equation is the assumption that the carrier population $N(r,z,t)$ instantaneously thermalizes within the valence band, thus permitting the absorption coefficient to be written as a product of the carrier concentration and the hole absorption cross section. However, carriers are injected via the TPA process into a narrow, nonthermal distribution of momentum states. These carriers thermalize within the band via carrier-carrier and carrier-phonon interactions. Previous experiments using time-resolved photoluminescence in GaAs indicate that these processes lead to carrier thermalization times of about 0.1–1 psec,¹¹ comparable to the optical pulse length used in our experiments. Thus, the assumption of a constant FCA coefficient is not strictly valid. A complete model must include the time dependence of the carrier distribution and thus the FCA absorption, and is beyond the scope of this paper. We emphasize that although the results of such a calculation would differ in detail from our simple analytical results, the general trends would remain unchanged.

With the assumption that the TPA coefficient β is a constant unaffected by saturation and carrier production, the carrier concentration $N(r, z, t)$ can be described by the following rate equation:

$$\frac{dN(r, z, t)}{dt} = \frac{\beta I^2(r, z, t)}{2\hbar\omega} - \eta N(r, z, t). \quad (6)$$

The coefficient η is the carrier relaxation rate, which can vary as a result of Auger recombination and impact ionization processes but should be nearly constant at low intensities.

With the assumption that $1/\eta \gg \tau$ (the optical pulse length), the second term in Eq. (6) can be ignored, and the remaining term integrated directly

$$N(r, z, t) = \int_{-\infty}^t \frac{\beta I^2(r, z, t')}{2\hbar\omega} dt'. \quad (7)$$

Using the results of Eqs. (5) and (7), Eq. (3) becomes

$$\begin{aligned} \frac{d}{dz} I(r, z, t) = & -\alpha_0 I(r, z, t) - \beta I^2(r, z, t) \\ & - \sigma_p I(r, z, t) \int_{-\infty}^t \frac{\beta I^2(r, z, t')}{2\hbar\omega} dt'. \end{aligned} \quad (8)$$

In principle, one can obtain a precise solution for $I(r, z, t)$ from the numerical solution of Eq. (8). However, we can take advantage of the fact that the final term, which represents the induced FCA contribution, can be ignored at low intensity. In this case, the remaining terms can be integrated analytically, yielding

$$I(r, z, t) = \frac{I_{\text{inc}}(r, t)(1-R)\alpha_0 e^{-\alpha_0 z}}{\alpha_0 + I_{\text{inc}}(r, t)(1-R)\beta(1-e^{-\alpha_0 z})} \quad (9)$$

where $I_{\text{inc}}(r, t)$ is the incident intensity, and R is the surface reflectivity of the sample, assumed to be constant.

Any real optical beam has both a transverse and a temporal variation in amplitude. We will consider beams that are nearly Gaussian in both spatial and temporal extent, and can therefore be described by $I_{\text{inc}}(r, t) = I_0 \exp(-2r^2/w_0^2 - t^2/\tau^2)$, where w_0 is the spatial width and τ is the temporal width. The transmitted energy is given by an integration over transverse space and time of the intensity profile at the exit of the sample. Performing all but the temporal integration, we can write the transmitted intensity in this compact form:

$$E_{\text{trans}} = \frac{I_0 \pi w_0^2 e^{-\alpha_0 d} (1-R)^2}{2\nu} \int_{-\infty}^{\infty} dt \ln[1 + \nu e^{-t^2/\tau^2}]. \quad (10)$$

Here d is the sample thickness, and $\nu \equiv \beta I_0 (1-R) (1 - e^{-\alpha_0 d}) / \alpha_0$ is a dimensionless parameter that is a measure of the strength of the TPA process. In the limit of no FCA, Eq. (10) is exact.

We can compute the integral in Eq. (10) by expanding the integrand, which unfortunately results in separate cases depending on whether ν is less than or greater than or equal to unity. For $\nu < 1$, after integrating term by term we find

$$E_{\text{trans}} = E_0 \sum_{n=1}^{\infty} \frac{\nu^{n-1} (-1)^{n-1}}{n^{3/2}}. \quad (11)$$

Here $E_0 = \frac{1}{2} \pi^{3/2} w_0^2 \tau I_0 (1-R)^2 e^{-\alpha_0 d}$ is the initial energy corrected for reflection losses and linear absorption. Since in the low-intensity limit we have $\nu < 1$, we can use Eq. (11) to fit the measured optical transmission. In particular, if we keep only the first two terms, we have a simple linear equation which can be fit to provide the linear absorption and TPA coefficients.

At higher intensities, when ν is equal to or larger than unity, the expansion in Eq. (11) does not converge. Using a different expansion we find that the transmitted energy can be written as

$$E_{\text{trans}} = E_0 \sum_{m=1}^{\infty} \sum_{n=0}^{m-1} \frac{(m-1)!}{n(m-n)!} \frac{(1-\nu)^n}{\nu^n} \frac{(-1)^{m+1}}{(m-n)^{3/2}}. \quad (12)$$

Once again, this equation is exact if FCA is ignored, and can therefore be used in the high-intensity limit to fit observed transmission curves to obtain both the linear and TPA absorption coefficients. Finally, we note that at $\nu=1$, both Eqs. (11) and (12) converge to the same value.

It is nonetheless still true that these solutions are valid only when the FCA is small compared to the TPA, and so it is important to verify that these conditions are maintained in an experiment. Using Eq. (8), we note that this is equivalent to requiring, for all t , that

$$\frac{\sigma_p I_0 (1-R)}{2\hbar\omega} \int_{-\infty}^t \exp\left[-2\left(\frac{t'}{\tau}\right)^2\right] dt' \ll 1. \quad (13)$$

The necessary condition for the intensity is then that $I_0 \ll 2\sqrt{2}\hbar\omega/\sigma_p \tau (1-R)$. For a 1-psec optical pulse at a wavelength of 6 μm , and assuming a free-hole absorption cross section of $5 \times 10^{-16} \text{ cm}^2$, this critical intensity is approximately 600 MW/cm^2 . This threshold intensity, although large, is readily achievable in practice, and thus it is important to limit analysis using Eqs. (11) and (12) to data obtained well below this value.

If we are careful to remain in this low-intensity limit, we can treat the FCA process as a perturbation, and consider introducing another term in the solution to Eq. (8) of the form $I_1(r, z, t) + \gamma I_2(r, z, t)$, where $\gamma = \sigma_p \beta / 2\hbar\omega$, and where I_1 is the solution without FCA given by Eq. (9). Inserting this trial function into Eq. (8), and keeping only lowest-order terms, we obtain the following differential equation for I_2 :

$$\frac{dI_2(r, z, t)}{dz} = -\alpha I_2(r, z, t) - \gamma I_1(r, z, t) \int_{-\infty}^t I_1^2(r, z, t') dt'. \quad (14)$$

This is a simple first-order differential equation; the solution $I_2(r, z, t)$ is given by this integral expression:

$$I_2(r, z, t) = e^{\alpha z} \int_0^z dz' e^{-\alpha z'} I_1(r, z', t) \int_{-\infty}^t dt' I_1^2(r, z', t'). \quad (15)$$

Although it is possible to solve Eq. (15) with the complete form of I_1 as given by Eq. (9), it is perhaps more instructive

to approximate I_1 with the input pulse, in which case our first-order perturbation takes a simple form:

$$I_2(r, z, t) = \frac{\gamma \tau \pi^{1/2} e^{-t^2/\tau^2} I_0^3 (1-R)^3 e^{-6r^2/w_0^2}}{6\sqrt{2}\alpha} (1 - e^{-3\alpha z}) \times [1 + \text{erf}(\sqrt{2t/\tau})]. \quad (16)$$

We can use this result to obtain the transmitted energy by integrating over the spatial and temporal extent of the pulse. We are left with the following expression for the energy:

$$E_2 = \frac{\tau^2 w_0^2 \gamma \pi^{3/2} (1 - e^{-3\alpha d}) (1-R)^4 I_0^3}{36\sqrt{2}\alpha} \int_{-\infty}^{\infty} e^{-t^2} \text{erf}(\sqrt{2t}) dt. \quad (17)$$

Once the TPA coefficient has been established using the low-intensity portion of the experimental data then Eq. (17) can be used to estimate σ_p , the free-hole absorption cross-section. By extending the perturbation expansion to higher order, we can fit the cross section to higher order in the intensity data, thereby attaining greater accuracy. We should note that in the work presented below we have in fact used a higher-order expansion, obtained by inserting the correct form of the intensity without FCA into Eq. (15) and integrating numerically.

IV. EXPERIMENTAL METHOD

Previous attempts to measure nonlinear absorption coefficients as a function of frequency have suffered in accuracy because of the cumulative uncertainties in pulse energy, spatial profile, and temporal shape.³ Furthermore, experiments performed as a function of wavelength suffer from variations in beam steering and focusing due to dispersion in the optical system. However, we see from Eq. (1) that the TPA coefficient depends not only on the photon energy but on the gap energy, which is strongly temperature dependent. For this study, therefore, we chose to vary the sample temperature. This method allowed us to measure the functional dependence of the TPA coefficient without varying any optical parameters, resulting in extremely high relative accuracy.

We used a single wafer of undoped InAs, 350 μm thick, optically polished on both sides. The sample was mounted on a variable temperature stage in a liquid-nitrogen-cooled cryostat, with the temperature feedback stabilized to better than 1 K. The FEL beam was focused to a spot onto the sample with an off-axis paraboloidal mirror. The spot size w_0 , measured with a pin hole, was less than 100 μm at all wavelengths. Some of the incident beam was diverted with a

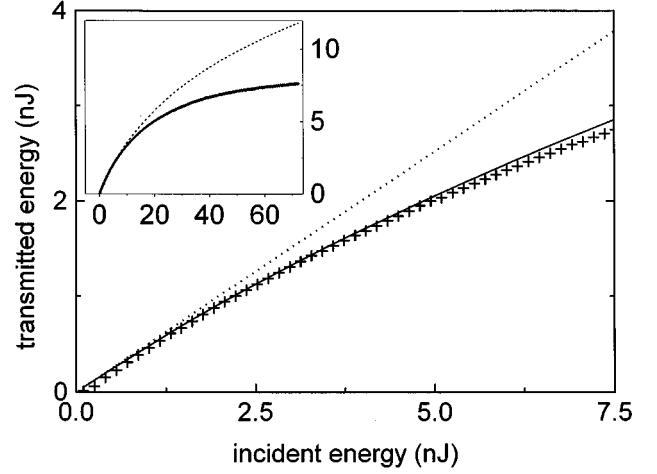


FIG. 2. Transmitted vs incident energy curve observed at 300 K, at 5.06 μm , demonstrating two-photon absorption. The dotted line is a linear calibration, while the solid line is a calculation using Eqs. (11) and (12). The inset shows the predicted curve and observed data at larger intensities, where higher-order absorption effects dominate.

beam splitter into a $\text{Hg}_x\text{Cd}_{1-x}\text{Te}$ detector calibrated by reference to a commercial pyrometer. Transmitted power was measured directly with an identical $\text{Hg}_x\text{Cd}_{1-x}\text{Te}$ detector.

The Stanford Picosecond FEL Center provides a near diffraction and transform-limited laser beam of “micropulses” repeating at 11.8 MHz within a “macropulse” of duration 3 ms and frequency 20 Hz. The capabilities of the Stanford FEL Center have been described in more detail elsewhere.¹² For our experiments, the micropulses had a Gaussian full width at half maximum of approximately 1 ps, which was continuously monitored with a separate autocorrelator. To eliminate the possibility of long-lived carrier or thermal effects, single optical micropulses were selected from the FEL pulse train with an acousto-optic modulator (AOM), which picked a single micropulse every 30 μs . Incident power was controlled by varying the rf power delivered to the AOM with a voltage controlled attenuator. The micropulse energy was effectively varied from 0–200 nJ. Boxcar averagers were used on the output of the detectors, which were then digitized by a computer data acquisition system. We emphasize that the power was varied and the data collected without any adjustment of optics, to prevent systematic steering or focusing errors.

From linear spectroscopy, we determined the variation of

TABLE I. Comparison of the measured absolute magnitude of the TPA coefficient with predictions from the three models at 5.06 and 6.3 μm . The sample temperature was 300 K in both cases.

| | Measurement wavelength | |
|---|------------------------|-----------------------|
| | 5.06 μm | 6.3 μm |
| Measured TPA coefficient | 0.89 ± 0.18 cm/MW | 0.69 ± 0.14 cm/MW |
| Parabolic band only | 1.94 | 0.93 |
| Nonparabolic model with no split-off band | 1.13 | 0.75 |
| Full model, including split-off band | 1.05 | 0.71 |

TABLE II. Comparison of the measured TPA coefficient with predictions from the three models. Each data set has been scaled by a single number of account for absolute uncertainty, and the values below are the resulting mean squared errors between data and prediction.

| Model | Comparison of mean squared error for each data set and model | | |
|---|--|----------------------|----------------------|
| | 4.55 μm | 5.06 μm | 6.3 μm |
| Parabolic band only | 1.7×10^{-4} | 1.1×10^{-2} | 5.6×10^{-4} |
| Nonparabolic model with no split-off band | 1.1×10^{-5} | 8.8×10^{-4} | 1.4×10^{-4} |
| Full model, including split-off band | 1.4×10^{-5} | 2.3×10^{-3} | 2.0×10^{-4} |

both the gap energy and the index of refraction with temperature, and we verified that the linear-absorption coefficient remained constant up to 350 K. Between 80 and 350 K the variation of the gap energy was linear according to $0.44 \text{ eV} - 0.00028 \text{ eV/K}$, in agreement with literature values.¹³ The index of refraction varied by about 5% across this temperature range.

V. EXPERIMENTAL RESULTS

We took data every five degrees from 80 to 350 K at three wavelengths 4.55, 5.06, and 6.3 μm . A typical data set, taken at 5.06 μm and 300 K is indicated in Fig. 2. The inset shows the full data set, which continues to intensities at which mechanisms other than TPA, particularly free-carrier absorption, become significant. We fit the data using the simple analytic expression for the transmitted energy described in Eq. (11), using data of sufficiently low intensity so that FCA was not significant. This method is in contrast to previous work⁴ that has relied on the saturation value of the transmission to infer the TPA coefficient.

With our fitting technique, the value of β obtained was then used to calculate the transmitted energy at higher intensities using the expansion in Eq. (12), which is exact in the limit of no FCA. The result of this calculation is shown by

the solid line in both the inset and the main figure. Note the upper axis of the figure, which displays the values for the parameter ν calibrated using the value of β obtained from the data. The dotted line represents the linear transmission of the sample in the absence of TPA.

At each wavelength and temperature we calculated the TPA coefficient by fitting the data set to Eq. (11). The relative value of the TPA coefficients determined at a single wavelength are substantially more accurate than the absolute value due to the intensity errors discussed previously. For this reason we have compared the TPA coefficient to the three theoretical models at each wavelength both in absolute magnitude and in functional form.

Using the measured values for the spot size, pulse length, sample thickness, and pulse energy, we calculated the absolute magnitude of the TPA coefficient at 6.3 and 5.06 μm (no independent calibration was made at 4.55 μm). Table I shows these data along with the corresponding predictions of the three theories. The data are in good agreement with the theory including nonparabolic contributions to the TPA coefficient, although the effect of the split-off band cannot be resolved within the measurement uncertainty.

Reaching agreement in absolute magnitude is important, but it is equally important to verify the functional form predicted by TPA. So using the photon energy and the known

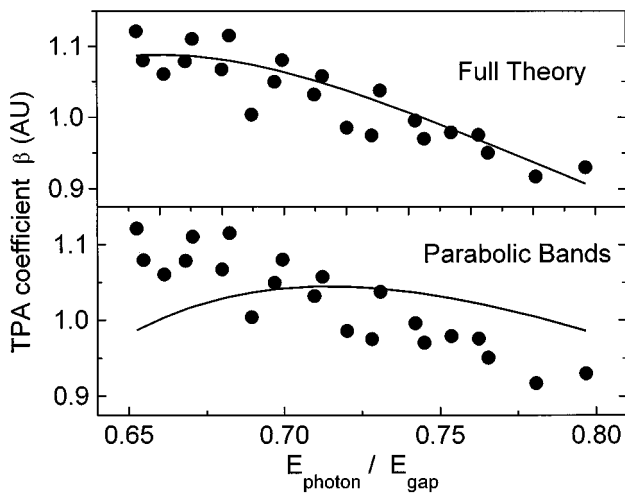


FIG. 3. Comparison of the experimental TPA coefficient with theoretical calculations at 4.55 μm ; (a) parabolic bands, (b) nonparabolic bands including split-off band, and nonzone center wave functions. The data set has been scaled by a single parameter to reach a best fit with the model to account for absolute uncertainty in the intensity measurement.

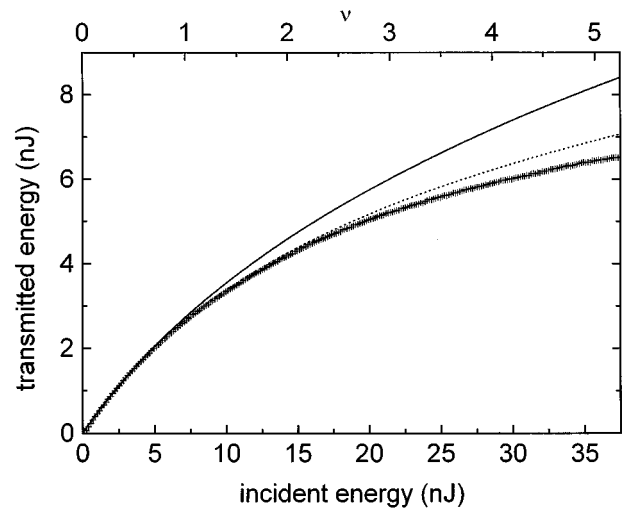


FIG. 4. Transmitted vs incident energy curve, again observed at 5.06 μm and 300 K as in Fig. 3. The dashed line shows the fit with both TPA and FCA included, while the solid line is a fit using only TPA for comparison. The top axis indicates the dimensionless intensity ν , as defined in Eq. (10).

TABLE III. Comparison of the measured FCA cross section σ_p to values obtained using linear spectroscopic techniques on p -doped InAs samples. The sample temperature was 300 K in both instances.

| | Hole absorption cross section σ_p (10^{-16} cm ²) | | |
|---|--|--------------|--------------|
| | 6.30 μ m | 5.06 μ m | 4.55 μ m |
| Present measurements | 6.0 | 11 | 11 |
| Linear spectroscopy on p -doped sample (3×10^{16} cm ³) | 8.2 | 5.0 | 2.0 |

temperature variation of the gap energy, we have compared the measured TPA coefficient at each wavelength to the three theoretical models. Because of the uncertainty in the absolute intensity, the data were adjusted to each theory curve by a single scaling parameter, and a minimum mean squared error was obtained. This process was repeated at each wavelength, with results summarized in Table II. It is clear that the parabolic model is ruled out, as it is in quantitative disagreement with the data. In Fig. 3 this is illustrated graphically with data taken at 4.55 μ m. This figure compares the best fits of this data set to both the parabolic model and the complete model, including split-off band. The only adjustment of the data between the two graphs is scaling by a constant factor to account for the absolute intensity measurement uncertainty.

According to Table II the present data are in better agreement when the split-off band is ignored. This may be due to insufficient modeling of the temperature dependence of the split-off energy, or other inadequacies of the theory. It is hoped that with further refinement the statistical errors can be reduced to provide further discrimination.

Having established the accuracy of nonparabolic theory of two-photon absorption, we may then use this theory to predict the FCA in the sample due to carriers produced in the TPA process. Figure 4 shows the same raw data in Fig. 2, in which the contributions of FCA have been included using a higher-order form of Eq. (17). The previous fit, without FCA, is also shown for purposes of comparison. It is clear that the agreement between data and fit is much better; however, the more complete theory still fails at higher intensities. This disagreement is to be expected, not only because Eq. (17) is a simple perturbation expansion, but also because several other physical processes can become important, including population dependence of the FCA cross section, nonlinear refraction, and carrier production by impact ionization. Since we have not attempted to model these processes, we restrict our attention to data at intensities low enough that the calculations presented here are more than adequate.

By fitting the transmitted energy curves we can obtain the FCA cross section σ_p for each temperature and excitation wavelength. Within about 15%, the results for σ_p obtained from the fitting process were constant with temperature. These results as a function of wavelength are summarized in Table III, along with previous linear spectroscopic studies of an equilibrium distribution of carriers.¹³

The experimental FCA cross section is in reasonable agreement with the previous measurements, providing good experimental verification of the carrier production and ab-

sorption models we have used here. Furthermore, much of the difference in observed cross sections between our results and earlier linear spectroscopic methods can be explained by the temperature of the carrier distributions we are probing. The effective temperature of carriers injected via the TPA process at 6.3 μ m is substantially lower than those injected at 4.55 μ m. At 300 K, in fact, the excess energy of the 6.3- μ m injected carriers amounts to 1.5 kT, while at 4.55 μ m this excess is 8 kT. A hot carrier distribution would be expected to exhibit stronger hole absorption, which is in agreement with our observations.

VI. CONCLUSIONS

We have performed a series of measurements at the Stanford Picosecond FEL Center to study the nonlinear absorption in InAs over a range of wavelengths and temperatures. The experiments were carefully constructed to eliminate any possible systematic error due to beam steering, sample heating, or long-lived carrier effects. By precise measurement of the transmitted energy as a function of incident energy, we can distinguish TPA from higher-order effects, such as TPA-induced FCA. The TPA coefficient derived in this way is in good agreement with theoretical calculations over a wide range in wavelength and temperature, and is able to distinguish nonparabolic effects in the calculations. This experiment has been able to discriminate, using measurements of the TPA coefficient, between calculations based on different band-structure models. We hope that by improving upon this technique we can provide more stringent tests of the TPA theory, in particular resolving effects due to the split-off band. In addition, we have studied the contribution of FCA to the sample absorption. Although the hole-absorption cross section agrees roughly with previous literature measurements, differences arise which may imply complex carrier dynamics. At still higher intensities, the theory based on TPA and FCA fails, indicating that higher-order absorption mechanisms are present, and can be studied in future work.

ACKNOWLEDGMENTS

The authors would like to thank T. I. Smith for suggesting this line of inquiry, and H. A. Schwettman for insight and beneficial criticism. This work was supported in part by the Office of Naval Research, Contracts Nos. N00014-91-C-0170 and N00014-94-1-1024.

- ¹For an introduction, see J. I. Pankove, *Optical Processes in Semiconductors* (Dover, New York, 1971).
- ²P. N. Butcher and D. Cotter, *The Elements of Nonlinear Optics* (Cambridge University Press, Cambridge, 1990), p. 246–274.
- ³E. W. Van Stryland and L. L. Chase, in *Handbook of Laser Science & Technology, Supplement 2: Optical Materials*, edited by Marvin J. Weber (CRC, Boca Raton, 1995), p. 299.
- ⁴B. N. Murdin *et al.*, *Opt. Quantum Electron.* **25**, 171 (1993).
- ⁵B. N. Murdin *et al.*, *Nucl. Instrum. Methods A* **341**, 165 (1994).
- ⁶R. J. Bakker, A. F. G. van der Meer, D. Oepts, and P. W. van Amersfoort, *Appl. Phys. Lett.* **61**, 2320 (1992).
- ⁷B. S. Wherrett, *J. Opt. Soc. Am. B* **1**, 67 (1984).
- ⁸M. H. Weiler, *Solid State Commun.* **39**, 937 (1981).
- ⁹D. C. Hutchings, and E. W. Van Stryland, *J. Opt. Soc. Am. B* **9**, 2065 (1992).
- ¹⁰R. B. James and D. L. Smith, *IEEE J. Quantum Electron* **QE-18**, 1841 (1982).
- ¹¹R. Rodrigues-Herzog *et al.*, *Appl. Phys. Lett.* **67**, 264 (1995).
- ¹²K. W. Berryman *et al.*, *Nucl. Instrum. Methods A* **358**, 300 (1995).
- ¹³F. Matossi and F. Stern, *Phys. Rev.* **111**, 472 (1958).